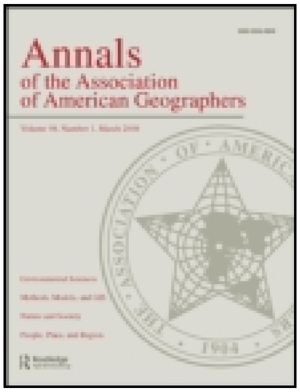

Annals of the Association of American Geographers
Publication details, including instructions for authors and subscription information:
http://www.tandfonline.com/loi/raag20

A Spatial-Temporal Modeling Approach to Reconstructing Land-Cover Change Trajectories from Multi-temporal Satellite Imagery

Desheng Liu [a] & Shanshan Cai [b]

[a] Department of Geography and Department of Statistics , The Ohio State University

[b] Department of Geography , The Ohio State University

Published online: 11 Aug 2011.

A Spatial-Temporal Modeling Approach to Reconstructing Land-Cover Change Trajectories from Multi-temporal Satellite Imagery

Desheng Liu* and Shanshan Cai†

*Department of Geography and Department of Statistics, The Ohio State University
†Department of Geography, The Ohio State University

Temporal trajectories of land-cover change provide important information on landscape dynamics that are critical to our understanding of complex human–environment adaptive systems. The increasing availability of long time series of satellite images, especially the recent free release of multi-decadal Landsat satellite archive, presents a great opportunity to improve our ability to detect land-cover change over multiple dates and advance land change science. In this article, a spatial-temporal modeling approach is developed for reconstructing land-cover change trajectories from time series of satellite images. The change detection method represents an enhancement to the conventional post-classification comparison. The key innovation lies in the use of Markov random field theory to model spatial-temporal contextual information explicitly in the classification of time series images. When evaluated using a time series of seven Landsat images in a case study of southeast Ohio, the spatial-temporal modeling approach yielded significantly more accurate and consistent trajectories of land-cover change than conventional non-contextual approaches. The results from the case study demonstrate the effectiveness of the change detection method in reconstructing land-cover change trajectories and also highlight the utility of spatial-temporal contextual information in improving the accuracy and consistency of land-cover classifications across space and time. *Key Words: change detection, land-cover change trajectories, Landsat imagery, post-classification comparison, spatial-temporal contextual information.*

土地覆盖变化的时空轨迹，给景观动态提供了重要信息，它对我们理解人类与环境的复杂自适应系统是至关重要的。长时间系列的卫星图像，特别是最近的多年地球资源卫星存档的免费发布，给提高我们检测多时次土地覆盖变化的能力和推进土地变化科学的发展，提供了一个很好的机会。在这篇文章中，我们开发了一个时空建模方法，从卫星图像的时间序列来重建土地覆盖变化的轨迹。此变化检测方法增强了传统的分类后比较法。关键创新在于用马尔可夫随机场理论来明确地模拟时间序列分类图中的时空背景信息。在俄亥俄州东南部的一个案例研究中，使用了由 7 个地球资源卫星图像组成的时间系列，该时空建模方法产生了比传统的非背景方法更为准确和一致的土地覆盖变化的轨迹。此案例研究的结果表明变化检测方法在重建土地覆盖变化轨迹中的有效性，也突出了时空背景信息在改善跨时空的土地覆盖分类的精确性和一致性上的效用。*关键词：变化检测，土地覆盖变化的轨迹，陆地卫星图像，分类后比较，时空的背景资料。*

Las trayectorias temporales de cambio de cobertura terrestre proporcionan información importante sobre la dinámica del paisaje que son fundamentales para nuestra comprensión de los complejos sistemas de adaptación humano-ambientales. La creciente disponibilidad de largas series temporales de imágenes de satélite, en especial el reciente libre lanzamiento de archivos de varios decenios del satélite Landsat, presentan una gran oportunidad para mejorar nuestra capacidad para detectar el cambio de la cobertura terrestre durante múltiples fechas y promover la ciencia del cambio de la tierra. En este artículo se ha desarrollado un enfoque de modelado espacio-temporal para reconstruir las trayectorias del cambio de cobertura terrestre de las series temporales de imágenes de satélite. El método de detección de cambio representa una mejora a la convencional comparación post-clasificación. La clave de la innovación radica en el uso de la teoría de campo aleatorio de Markov para modelar información contextual espacial-temporal de forma explícita en la clasificación de imágenes de series de tiempo. Cuando se evaluó utilizando una serie de tiempos de siete imágenes Landsat en un caso de estudio del sureste de Ohio, el enfoque del modelo espacio-temporal produjo trayectorias mucho más precisas y coherentes del cambio de la cobertura terrestre que los enfoques convencionales no contextuales. Los resultados del caso de estudio demuestran la eficacia del método de detección de cambios en la reconstrucción de trayectorias de cambios de cobertura terrestre y también resaltan la utilidad de la información contextual espacio-temporal en la mejora de la precisión y coherencia de las clasificaciones de la cobertura terrestre a través del espacio y del tiempo.

Annals of the Association of American Geographers, 102(6) 2012, pp. 1329–1347
Initial submission, September 2010; revised submission, December 2010; final acceptance, February 2011
Published by Taylor & Francis, LLC.

Palabras claves: detección de cambios, trayectorias de cambio de cobertura terrestre, imágenes Landsat, comparación post-clasificación, información contextual espacio-temporal.

With the increased pace, extent, and intensity of human alterations of the Earth's land surface, the last several decades have witnessed unprecedented land-use and land-cover change (LULCC) at a broad range of spatial and temporal scales (Turner et al. 1990; Meyer 1994; Steffen et al. 2004). The dramatic changes in land use and land cover impact the Earth system in myriad ways, including global climate change, loss of biodiversity, and soil degradation, among others (Vitousek et al. 1997; Lambin et al. 1999; Foley et al. 2005). Understanding the spatial and temporal dynamics of LULCC, its natural and anthropogenic causes, and its potential impacts and consequences is crucial to sustainable human development, and has thus received great attention from various research communities, leading to the emergence of a new interdisciplinary research field, increasingly referred to as *land change science* (Rindfuss et al. 2004; Turner, Lambin, and Reenberg 2007).

Remote Sensing of Land-Cover Change

One critical component of land change science is the observation and monitoring of land-cover change at various spatial and temporal scales (Rindfuss et al. 2004; Turner, Lambin, and Reenberg 2007). Although traditional field-based approaches can provide detailed and spatially disaggregated information on land-cover change, they are limited by their spatial extent and temporal frequency (Petit, Scudder, and Lambin 2001). In this regard, satellite remote sensing has been playing a major role in land-cover change monitoring due to its capability to observe the land surface in a repetitive and consistent manner over large areas. In particular, the Earth-observing satellite missions of the Landsat program have been acquiring time series of satellite imagery of the Earth every sixteen to eighteen days since 1972 (U.S. Geological Survey [USGS] 2003), providing the longest satellite records on land-cover dynamics over the past four decades throughout the world (Williams, Goward, and Arvidson 2006). The unparalleled temporal span of the Landsat time series together with its relatively sufficient spatial resolution and spectral coverage have made it the most widely used satellite data in LULCC studies (Goward and Williams 1997; Cohen and Goward 2004).

Despite the great potential offered by the long time series of Landsat imagery, most LULCC studies only use a pair of Landsat images acquired at two points in time for land-cover change detection and modeling (Mertens and Lambin 2000; Kennedy, Cohen, and Schroeder 2007; Mena 2008; Huang et al. 2010). This bi-temporal change analysis is sufficient for LULCC studies focusing on the rate and spatial pattern of net change in a given time period. More often than not, however, the transition process underlying land-cover change is of more interest because it is critical to understand when and how human impacts alter the landscapes (Mertens and Lambin 2000; Petit, Scudder, and Lambin 2001; An and Brown 2008; Mena 2008). As an emergent property of coupled human–environment systems, land-cover change, especially over a long time period, often follows nonlinear, reversible, and time-varying pathways that are too complex to be represented by observations at two dates (Mertens and Lambin 2000; Braimoh and Vlek 2005). For example, Vågen (2006) found a complex nonlinear temporal pattern of deforestation in Madagascar using a time series of Landsat images acquired on five different dates and concluded that such patterns would not have been seen if observations from only two dates had been used. Similarly, Mertens and Lambin (2000) developed a multivariate spatial model of satellite-derived land-cover change trajectories associated with different deforestation processes in southern Cameroon. Their results showed that modeling land-cover change trajectories over several observation years improved the projection of areas with a high probability of change over projections based on observations from only the previous period alone. Therefore, temporal sequences of land-cover classes derived from satellite images at multiple dates (i.e., more than two dates), henceforth called *land-cover change trajectories* (Mertens and Lambin 2000), are needed for better characterization of land-cover dynamics of complex human–environment adaptive systems.

The concept of multi-temporal land-cover change trajectory analysis is obviously not new (see Lambin 1997; Mertens and Lambin 2000), but its applications in LULCC studies have not been widely explored compared with traditional bi-temporal land-cover change analysis. This has perhaps been in part due to the limited access to a longer satellite time series, especially Landsat data. The recent opening of the Landsat archive to the public for free Web-based access has greatly improved the accessibility of multi-temporal Landsat data (USGS 2008), opening up an unprecedented opportunity to advance land-cover change trajectory analysis for LULCC studies. It is anticipated that there will be growing interest from the land change science community in making use of the freely available multi-temporal Landsat data to analyze the trajectories of land-cover change over the past decades. Due to the complex nature of land-cover dynamics, however, challenges remain in the accurate reconstruction of land-cover change trajectories from multi-temporal satellite imagery. To meet the increasing need for change trajectory analysis, change detection techniques based on multi-temporal satellite imagery must be advanced accordingly.

Multi-temporal Change Detection Techniques

Many computer techniques have been developed for detecting land-cover change using satellite data during the past three decades. Summaries of existing change detection techniques can be found in numerous review papers, such as Coppin et al. (2004), Lu et al. (2004), and Singh (1989). Due to the dominance of bi-temporal change analysis, most of these techniques are developed for detecting changes using images at two dates only (Coppin et al. 2004; Kennedy, Cohen, and Schroeder 2007; Huang et al. 2010). By contrast, techniques designed for multi-temporal change analysis using images at more than two dates are much fewer and largely limited to two groups: (1) temporal trajectory analysis of satellite imagery time series and (2) multi-temporal post-classification comparison.

Temporal trajectory analysis detects changes directly by modeling temporal signatures of change processes of interest using the time profiles of high-temporal-frequency satellite data such as Advanced Very High Resolution Radiometry (AVHRR) and Moderate Resolution Imaging Spectrometry (MODIS; Myneni et al. 1997; Coppin et al. 2004; Lunetta et al. 2006). This technique is particularly useful for detecting subtle seasonal and interannual changes in ecosystem properties that are not easily discernable by bi-temporal change detection techniques (Coppin et al. 2004; Kennedy, Cohen, and Schroeder 2007). Recently, trajectory-based change detection techniques have been developed to monitor forest disturbance history using dense Landsat time series (Kennedy, Cohen, and Schroeder 2007; Huang et al. 2010). However, the time profile–based technique is mainly restricted to a few specific change processes with characteristic temporal signatures at large spatial scales (e.g., forest disturbance and vegetation dynamics; Coppin et al. 2004), so it is not suitable for detecting a potentially large number of general transitions between different land-cover classes over time.

On the other hand, post-classification comparison first classifies multi-temporal satellite images into land-cover classes independently at each date and then compares the classified land-cover sequences successively to construct the trajectories of land-cover change. In contrast with temporal trajectory analysis, post-classification comparison is typically applied to higher spatial resolution imagery (e.g., Landsat imagery) to generate detailed change transitions between different land-cover classes. This technique was initially developed to detect land-cover transitions between two dates (i.e., the "from–to" land-cover changes), and its extension to more than two dates represents a natural way to track land-cover change trajectories over multiple dates.

To date, post-classification comparison has been used predominantly for reconstructing land-cover change trajectories in various LULCC studies (e.g., Lucas et al. 1993; Alves and Skole 1996; Mertens and Lambin 2000; Petit, Scudder, and Lambin 2001; Southworth et al. 2004; Braimoh and Vlek 2005; Mena 2008; Kuemmerle et al. 2009). It is well known, however, that the accuracy of post-classification comparison is highly dependent on the land-cover classification results at each date (Coppin et al. 2004). By its very nature, land-cover classification from satellite imagery inherently possesses various classification errors caused by factors such as noise in satellite observations, spectral confusion among different land-cover classes, and limitations of classification algorithms. Consequently, when multi-temporal land-cover results of the same area are combined, classification errors generated at each date will inevitably be propagated to the post-classification comparison process, potentially leading to poor accuracy in the resulting change trajectories (Singh 1989; Foody 2002). This issue becomes increasingly more critical as longer time series of satellite images are involved in post-classification comparison. Therefore, to achieve sufficient accuracy on land-cover change trajectories, accurate and consistent land-cover classification results across space and time are needed for multi-temporal post-classification comparison. To this end, spectral information directly from satellite observations is usually not enough, and the spatial and temporal context related to land-cover change trajectories must be incorporated in the classification (Boucher, Seto, and Journel 2006; D. S. Liu, Kelly, and Gong 2006; D. S. Liu et al. 2008; Powell et al. 2008; D. S. Liu and Chun 2009).

The purpose of this article is to develop an advanced change detection method based on post-classification comparison for reconstructing land-cover change trajectories from multi-temporal satellite imagery. Current approaches for post-classification comparison have proven to be substantially affected by error propagation due to their ignorance of important spatial-temporal context of land-cover change trajectories (D. S. Liu and Chun 2009). In this article, we present a novel spatial-temporal modeling approach for post-classification comparison to minimize error propagation in post-classification comparison and improve the accuracy of land-cover change trajectories. Specifically, a spatial-temporal contextual classification model is developed to exploit the use of spatial-temporal contextual information in improving land cover classifications over multiple dates. This spatial-temporal contextual classification model extends the previous work by D. S. Liu, Kelly, and Gong (2006) and D. S. Liu et al. (2008) for land-cover change detection at two dates to multiple dates for detecting land-cover change trajectories.

The rest of the article is organized as follows. We first present basic notations and lay out the change detection problem. We then introduce in detail an advanced change detection method in which spatial-temporal contextual information is modeled for better mapping of land-cover change trajectories. After that, we apply the change detection method to a case study of land-cover change in southeast Ohio, where complex trajectories of land-cover change associated with secondary forest succession have been observed. To evaluate the method, we compare it with conventional non-contextual change detection methods and demonstrate the values of spatial-temporal contextual information in change detection. Finally, we conclude the article with discussions on some critical issues in land-cover change detection.

Problem Statement

Suppose a time series of remote sensing images has been acquired in the study area of interest at m ($m > 2$) different dates. The time series of images are assumed to have been well registered to each other. Let each pixel in the image time series be referenced by a pair of indexes (s, t), where s is an index of spatial location and $s \in \mathbb{S} = \{1, \ldots, n\}$, with n being the total number of pixels in each image; t is an index of time and $t \in \mathbb{T} = \{1, \ldots, m\}$. Let the multi-temporal images be denoted by $\boldsymbol{X} = \{X_{(s,t)} | s \in \mathbb{S}, t \in \mathbb{T}\}$, where $X_{(s,t)}$ represents the observed spectral data of pixel (s, t). Let the underlying multi-temporal land-cover process be denoted by $\boldsymbol{L} = \{L_{(s,t)} | s \in \mathbb{S}, t \in \mathbb{T}\}$, where $L_{(s,t)}$ represents the class label of pixel (s, t) and belongs to one of k land-cover classes $\{l_1, \ldots, l_k\}$.

Our goal is to reconstruct the trajectories of land-cover change over the m dates at each pixel location s ($s \in \mathbb{S}$), $L_{(s,1)} \rightarrow \cdots \rightarrow L_{(s,m)}$, from the observed multi-temporal image data set $\boldsymbol{X}$. To this end, the most straightforward approach is post-classification comparison, by which land-cover change trajectories can be easily established from land-cover classification maps at different dates. Given this, our problem is essentially one of multi-temporal land-cover classification. That is, to generate the land-cover change trajectories at all pixel locations, we need to map the underlying multi-temporal land-cover process $\boldsymbol{L}$ through the classification of the multi-temporal images $\boldsymbol{X}$.

In a Bayesian framework, the optimal classification of multi-temporal images $\boldsymbol{X}$ is determined by the maximum a posteriori (MAP) classification rule,

$$\boldsymbol{L}^* = \arg\max_{\boldsymbol{L}}\{P(\boldsymbol{L}|\boldsymbol{X})\}, \tag{1}$$

where $\boldsymbol{L}^*$ denotes the MAP estimate of the multi-temporal land-cover process; $P(\boldsymbol{L}|\boldsymbol{X})$ is the posterior probability of the land-cover process $\boldsymbol{L}$ given the data $\boldsymbol{X}$; and $\arg\max_{\boldsymbol{L}}\{P(\boldsymbol{L}|\boldsymbol{X})\}$ stands for the multi-temporal classification that maximizes the posterior probability.

Solving Equation 1 involves two tasks: modeling the posterior probability distribution and searching for the MAP solution using an optimization algorithm, both of which are difficult due to the complex spatial-temporal structure (i.e., spatial-temporal dependence) of the multi-temporal images and the land-cover process. To simplify the model specification and optimization, most LULCC studies do not consider the spatial-temporal structure and conveniently assume spatial-temporal independence among pixels, with which the joint multi-temporal land-cover classification can be decomposed into independent land-cover classification at each pixel. This leads to a non-contextual classification model in which the class label of each pixel is solely determined by its spectral information. The MAP classification rule in Equation 1 for the non-contextual model is then reduced to

$$L^*_{(s,t)} = \arg\max_{L_{(s,t)}} \left\{ P\left(L_{(s,t)} \middle| X_{(s,t)} \right) \right\}; \quad \text{for } s \in \mathbb{S}, t \in \mathbb{T}. \tag{2}$$

Although the non-contextual approach to multi-temporal land-cover classification is conceptually simple and computationally appealing, the important spatial-temporal context related to land-cover change trajectories is completely discarded in the classification. In the next section, we present a novel spatial-temporal modeling approach to the stated classification problem to improve the accuracy and consistency of land-cover change trajectories.

Methods

MAP-MRF Classification Framework

In contrast to the conventional non-contextual classification model that uses spectral information only, a spatial-temporal contextual classification model is developed in this article to integrate both spectral information and spatial-temporal contextual information in the classification. Using Bayes's theorem, the MAP classification rule in Equation 1 can be written as:

$$\boldsymbol{L}^* = \arg\max_{\boldsymbol{L}} \left\{ P(\boldsymbol{L}) \times \ell(\boldsymbol{X}|\boldsymbol{L}) \right\}, \tag{3}$$

where $P(\boldsymbol{L})$ is the prior probability of the land-cover process $\boldsymbol{L}$; and $\ell(\boldsymbol{X}|\boldsymbol{L})$ is the likelihood of the data $\boldsymbol{X}$ given $\boldsymbol{L}$. Equation 3 provides a generative modeling framework to our classification problem that allows us to model spectral information and spatial-temporal contextual information separately.

The prior probability $P(\boldsymbol{L})$ takes into account our a priori knowledge about the spatial-temporal context of the underlying land-cover process. Markov random field (MRF) theory provides a convenient and consistent approach to modeling such contextual relationships through characterizing local statistical dependences among image pixels in terms of conditional prior distributions (Besag 1986; Dubes and Jain 1989; Cressie 1993; Li 2001). As such, we develop a three-dimensional MRF model to account for the spatial-temporal dependences of the underlying land-cover process (Solberg, Taxt, and Jain 1996; Melgani and Serpico 2003; D. S. Liu, Kelly, and Gong 2006; D. S. Liu et al. 2008). To do so, it is necessary to define a neighborhood system on which the spatial-temporal contextual dependences will be established. For this purpose, we define a second-order spatial-temporal neighborhood system (Figure 1) by extending the neighborhood system defined at two dates in D. S. Liu, Kelly, and Gong (2006) to multiple dates. As illustrated in Figure 1, the neighbors of pixel (s, t), denoted by $\mathbb{N}(s, t)$, consist of a subset of spatial-temporally adjacent pixels around the pixel. Given the defined neighborhood system, the land-cover process $\boldsymbol{L}$ is said to be a three-dimensional MRF if the conditional distribution of the land-cover class at an arbitrary pixel (s, t) given all other pixels in the multi-temporal images is only dependent on its spatial-temporal neighbors for all $s \in \mathbb{S}$ and $t \in \mathbb{T}$:

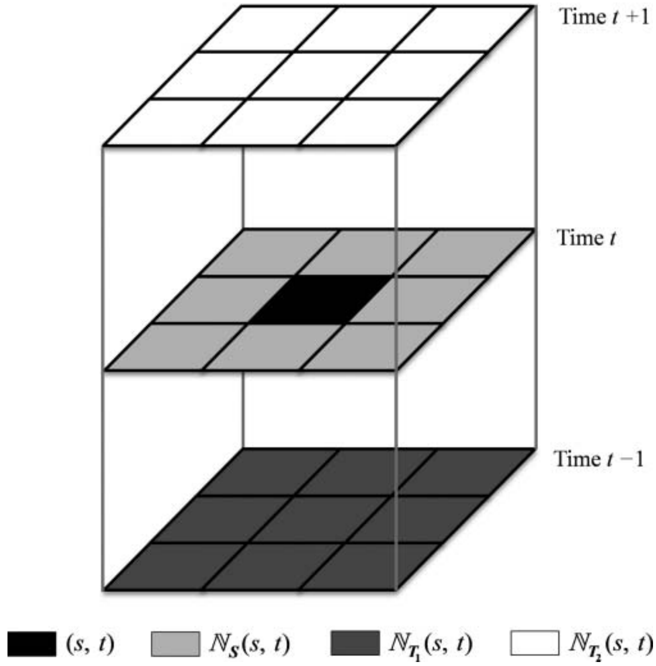

Figure 1. The spatial-temporal neighborhood system used in the Markov random field (MRF) model. The spatial-temporal neighbors of pixel(s, t), $\mathbb{N}(s, t)$, include (1) spatial neighbors, $\mathbb{N}_S(s, t)$, (2) past temporal neighbors, $\mathbb{N}_{T_1}(s, t)$, and (3) future temporal neighbors, $\mathbb{N}_{T_2}(s, t)$.

$$P\left(L_{(s,t)} \middle| \boldsymbol{L}_{-(s,t)} \right) = P\left(L_{(s,t)} \middle| \boldsymbol{L}_{\mathbb{N}(s,t)} \right), \tag{4}$$

where $\boldsymbol{L}_{-(s,t)} = \{L_{(s',t')} | (s', t') \neq (s, t)\}$ represents the class labels of all pixels other than pixel (s, t); and $\boldsymbol{L}_{\mathbb{N}(s,t)} = \{L_{(s',t')} | (s', t') \in \mathbb{N}(s, t)\}$ represents the class labels of all spatial-temporal neighbors of pixel (s, t). Based on the Hammersley–Clifford theorem (Hammersley and Clifford 1971), the joint distribution of an MRF is a Gibbs distribution defined on the same neighborhood system:

$$P(\boldsymbol{L}) = \frac{1}{Z} \exp\left[-U(\boldsymbol{L})\right] = \frac{1}{Z} \exp\left[-\sum\nolimits_{c \in \mathbb{C}} V_c(\boldsymbol{L}_c) \right], \tag{5}$$

where $\mathbb{Z}$ is a normalizing constant called the partition function; $U(\boldsymbol{L})$ is called the energy function; c is a clique;[1] $\mathbb{C}$ is the set of all cliques; $\boldsymbol{L}_c$ is the value of $\boldsymbol{L}$ at the pixels in clique c; and $V_c(\boldsymbol{L}_c)$ is the potential function of $\boldsymbol{L}_c$. Equation 5 provides a simple form to specify the joint distribution of an MRF in terms of the clique potential functions $V_c(\boldsymbol{L}_c)$ in the corresponding Gibbs distribution.

The likelihood function $\ell(\boldsymbol{X}|\boldsymbol{L})$ represents the contribution of observed spectral data to the land-cover classification. Given that the spatial-temporal dependence among image pixels is modeled through the prior distribution $P(\boldsymbol{L})$ using MRF theory, we assume conditional independence for $\ell(\boldsymbol{X}|\boldsymbol{L})$ to simplify the model specification (Besag 1986). Consequently, the likelihood function is modeled as the product of the marginal likelihood function at each pixel:

$$\ell(\boldsymbol{X}|\boldsymbol{L}) = \prod_{t=1}^{m}\prod_{s=1}^{n} f\left(X_{(s,t)}\,|L_{(s,t)}\right), \tag{6}$$

where $f(X_{(s,t)}|L_{(s,t)})$ is the marginal likelihood function at pixel (s, t).

With Equations 5 and 6, we obtain a mathematically tractable MAP-MRF framework for Equation 3 to model the joint multi-temporal land-cover classification with integrated use of spectral information and spatial-temporal contextual information (Li 2001). The MAP solution, however, is computationally prohibitive to obtain due to the combinatorial nature of the joint optimization over all possible values of $\boldsymbol{L}$. To simplify the optimization, we use a computationally feasible algorithm called *iterated conditional modes* (ICM) to approximate the MAP solution (Besag 1986). Instead of maximizing the joint posterior probability over all image pixels simultaneously, ICM maximizes the conditional posterior probability of each pixel sequentially:

$$\begin{aligned} L^*_{(s,t)} &= \arg\max_{L_{(s,t)}}\left\{P\left(L_{(s,t)}\,|X_{(s,t)}, \boldsymbol{L}_{\mathbb{N}(s,t)}\right)\right\} \\ &= \arg\max_{L_{(s,t)}}\left\{f\left(X_{(s,t)}\,|L_{(s,t)}\right)\times P\left(L_{(s,t)}\,|\boldsymbol{L}_{\mathbb{N}(s,t)}\right)\right\}. \end{aligned} \tag{7}$$

The conditional prior distribution $P(L_{(s,t)}|\boldsymbol{L}_{\mathbb{N}(s,t)})$ can be easily derived from Equation 5 (Li 2001):

$$\begin{aligned} P\left(L_{(s,t)}\,|\boldsymbol{L}_{\mathbb{N}(s,t)}\right) &= \frac{1}{\mathbb{Z}_{(s,t)}}\exp\left[-U\left(L_{(s,t)}\,|\boldsymbol{L}_{\mathbb{N}(s,t)}\right)\right] \\ &= \frac{1}{\mathbb{Z}_{(s,t)}}\exp\left[-\sum\nolimits_{c\in\mathbb{C}(s,t)} V_c(\boldsymbol{L}_c)\right], \end{aligned} \tag{8}$$

where $U(L_{(s,t)}|\boldsymbol{L}_{\mathbb{N}(s,t)})$ is the spatial-temporal energy function at the pixel (s, t), which will be specified in the following section; $\mathbb{C}(s, t)$ is the set of cliques containing pixel (s, t); and $\mathbb{Z}_{(s,t)}$ is a normalizing constant.

It should be noted that the classification of each pixel in Equation 7 depends on the class labels of its neighboring pixels, the classifications of which further depend on their neighboring pixels. The class labels of the neighboring pixels of all pixels are not available at the beginning of the classification, however, and must be estimated to solve Equation 7. ICM uses an iterative approach to obtain the estimates of all class labels. Specifically, the class labels at all pixels are initially estimated using the non-contextual model as outlined in Equation 2. This generates the initial spatial-temporal neighbors, from which ICM proceeds to update the classification based on Equation 7 until convergence is reached. Because the results of ICM are highly dependent on the initial classification, we use a competitive machine learning algorithm, support vector machines (SVM), to obtain the initial class labels and the likelihood estimate as suggested by D. S. Liu, Kelly, and Gong (2006). Figure 2 provides a flowchart for the ICM scheme to the MAP-MRF classification framework.

Specification of Spatial-Temporal Energy Functions

To model the varying statistical dependence of pixel (s, t) on its spatial-temporal neighbors, pixels in $\mathbb{N}(s, t)$ are divided into three mutually exclusive subsets (Figure 1): (1) spatial neighbors, denoted by $\mathbb{N}_{\boldsymbol{S}}(s, t)$; (2) past temporal neighbors,[2] denoted by $\mathbb{N}_{\boldsymbol{T}_1}(s, t)$; and (3) future temporal neighbors,[3] denoted by $\mathbb{N}_{\boldsymbol{T}_2}(s, t)$. The total spatial-temporal energy function $U(L_{(s,t)}|\boldsymbol{L}_{\mathbb{N}(s,t)})$ in Equation 8 is then modeled as the sum of three energy functions associated with the three subsets of neighbors:

$$\begin{aligned} U\left(L_{(s,t)}\,|\boldsymbol{L}_{\mathbb{N}(s,t)}\right) &= U_{\boldsymbol{S}}\left(L_{(s,t)}\,|\boldsymbol{L}_{\mathbb{N}_{\boldsymbol{S}}(s,t)}\right) \\ &\quad + U_{\boldsymbol{T}_1}\left(L_{(s,t)}\,|\boldsymbol{L}_{\mathbb{N}_{\boldsymbol{T}_1}(s,t)}\right) + U_{\boldsymbol{T}_2}\left(L_{(s,t)}\,|\boldsymbol{L}_{\mathbb{N}_{\boldsymbol{T}_2}(s,t)}\right), \end{aligned} \tag{9}$$

where $U_{\boldsymbol{S}}$ is the spatial energy function, and $U_{\boldsymbol{T}_1}$ and $U_{\boldsymbol{T}_2}$ are the past and future temporal energy functions, respectively. According to Equation 8, specifying the spatial-temporal energy function amounts to defining the corresponding clique potential functions. For computational and mathematical convenience, we define homogenous potential functions for cliques of size two (i.e., a clique consists of only two neighboring pixels; see Li 2001). Therefore, the spatial and temporal energy

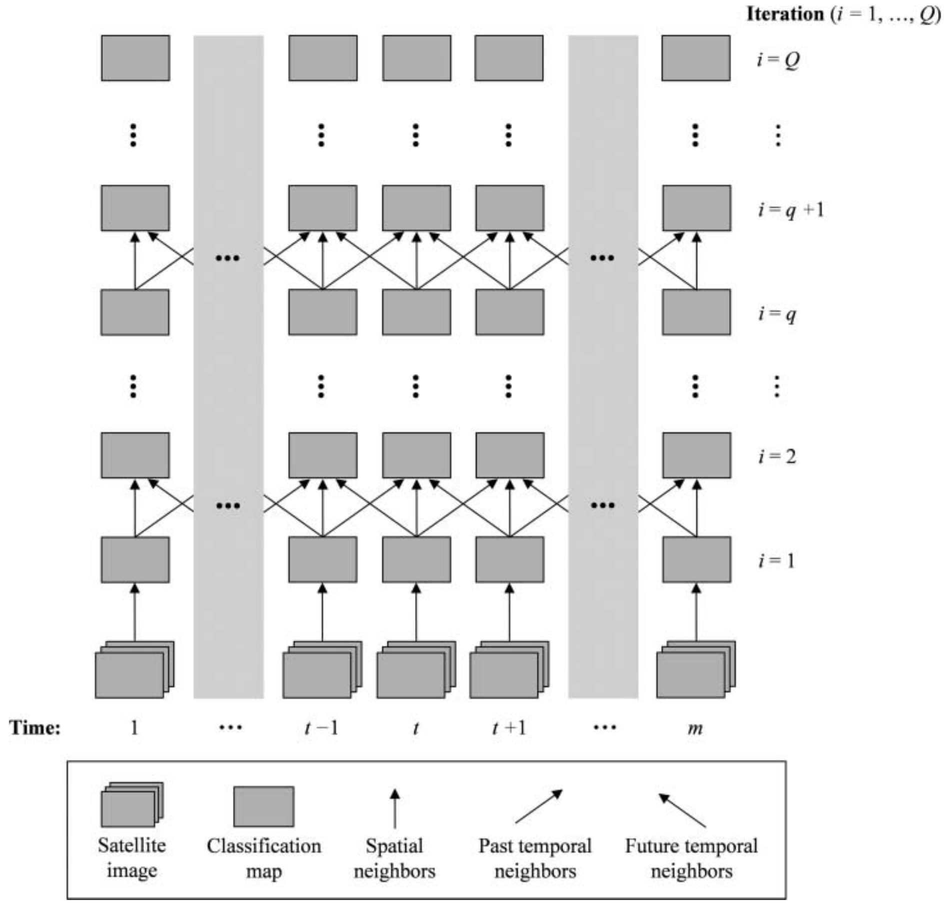

Figure 2. Flowchart of the iterated conditional modes (ICM) scheme to the maximum a posteriori-Markov random field (MAP-MRF) classification framework. The classification is initialized ($i = 1$) by Support Vector Machines (SVM) using spectral information only and then updated iteratively with estimated contextual information ($i = 2 \ldots$) until convergence between two iterations is reached ($i = Q$). The spatial-temporal neighbors at an arbitrary iteration ($i = q + 1$) are from the classification maps in the previous iteration ($i = q$).

functions in Equation 9 are specified in the following as the sum of pairwise potential functions of pixel (s, t) and its neighboring pixels within the respective neighborhood subset.

The spatial energy function in Equation 9 models the dependence of the land-cover classes of spatially neighboring pixels. Given that pixels adjacent to each other tend to come from the same land-cover class, the spatial energy function is specified to encourage assigning the same class labels to spatially neighboring pixels. This essentially imposes a spatial smoothness effect on the classification, which can reduce the speckle errors inherent in non-contextual classification models and thus mitigate error propagation in post-classification comparison. Specifically, the spatial energy function is characterized by the agreement in class labels between each pixel and its spatial neighbors:

$$U_S\left(L_{(s,t)}\,\middle|\,\boldsymbol{L}_{\mathbb{N}_S(s,t)}\right) = \sum\nolimits_{(s',t')\in\mathbb{N}_S(s,t)} V_S\left(L_{(s,t)}, L_{(s',t')}\right);$$
$$V_S\left(L_{(s,t)}, L_{(s',t')}\right) = -\beta_1 I\left(L_{(s,t)} = L_{(s',t')}\right), \qquad (10)$$

where $V_S(L_{(s,t)}, L_{(s',t')})$ is the pairwise potential function of pixel (s, t) and its spatial neighbor (s', t'); β_1 is a nonnegative parameter controlling the significance of spatial dependence; and $I(L_{(s,t)} = L_{(s',t')})$ is an indicator function that is equal to 1 if $L_{(s,t)} = L_{(s',t')}$ is true and 0 otherwise.

The two temporal energy functions in Equation 9 model the dependence of land-cover classes of temporally neighboring pixels. As a crucial component of multi-temporal land-cover classification, temporal dependence plays an important role in reconstructing land-cover change trajectories. In this article, we consider two types of temporal dependence: temporal relation and temporal exclusion. Temporal relation models the general dependence structure based on transition probabilities of land-cover classes from one date to another date, which permits the exchange of temporal information in the classification and thus links land-cover classifications at two consecutive dates. One common consequence of error propagation in post-classification comparison, however, is the occurrence of illogical land-cover transitions in resulting land-cover change trajectories. For example, a transition from urban to crop is unlikely in most situations, and a transition from grass to forest would not occur in a short time period. Therefore, temporal exclusion is used to model the negative dependence such that the occurrence of illogical land-cover transitions between temporally neighboring pixels will induce a penalty in terms of an increase in the temporal energy function (D. S. Liu, Kelly, and Gong 2006). This will greatly reduce illogical transitions in the final land-cover change trajectories. Specifically, the past temporal energy function $U_{\mathbf{T}_1}$ is characterized by:[4]

$$\begin{aligned} &U_{\mathbf{T}_1}\left(L_{(s,t)} \left| \boldsymbol{L}_{\mathbb{N}_{T_1}(s,t)}\right.\right) \\ &\quad = \sum\nolimits_{(s',t')\in\mathbb{N}_{T_1}(s,t)} V_{\mathbf{T}_1}(L_{(s,t)}, L_{(s',t')}); \\ &V_{\mathbf{T}_1}(L_{(s,t)}, L_{(s',t')}) = -\beta_2 P\left(L_{(s,t)} \left| L_{(s',t')}\right.\right) \\ &\quad + \beta_3 I(L_{(s',t')} \not\Rightarrow L_{(s,t)}), \end{aligned} \tag{11}$$

where $V_{\mathbf{T}_1}(L_{(s,t)}, L_{(s',t')})$ is the pairwise potential function of pixel (s, t) and its past temporal neighbor (s', t'); β_2 and β_3 are nonnegative parameters controlling the temporal relation and temporal exclusion, respectively; $P(L_{(s,t)}|L_{(s',t')})$ is the temporal transition probability from class $L_{(s',t')}$ to class $L_{(s,t)}$ that can be estimated by methods developed in D. S. Liu et al. (2008); and $I(L_{(s',t')} \not\Rightarrow L_{(s,t)})$ is an indicator function that is equal to 1 if the transition from $L_{(s',t')}$ to $L_{(s,t)}$ is illogical and 0 otherwise. The illogical transitions can be defined by expert knowledge (H. Liu and Zhou 2004; D. S. Liu, Kelly, and Gong 2006; Townsend et al. 2009). In the same vein, the future temporal energy function $U_{\mathbf{T}_2}$ is characterized by[5]:

$$\begin{aligned} &U_{\mathbf{T}_2}\left(L_{(s,t)} \left| \boldsymbol{L}_{\mathbb{N}_{T_2}(s,t)}\right.\right) \\ &\quad = \sum\nolimits_{(s',t')\in\mathbb{N}_{T_2}(s,t)} V_{\mathbf{T}_2}(L_{(s,t)}, L_{(s',t')}); \\ &V_{\mathbf{T}_2}(L_{(s,t)}, L_{(s',t')}) = -\beta_4 P\left(L_{(s',t')} \left| L_{(s,t)}\right.\right) \\ &\quad + \beta_5 I(L_{(s,t)} \not\Rightarrow L_{(s',t')}), \end{aligned} \tag{12}$$

where $V_{\mathbf{T}_2}(L_{(s,t)}, L_{(s',t')})$ is the pairwise potential function of pixel (s, t) and its future temporal neighbor (s', t'); β_4 and β_5 are nonnegative parameters controlling the temporal relation and temporal exclusion, respectively; and $P(L_{(s',t')}|L_{(s,t)})$ and $I(L_{(s,t)} \not\Rightarrow L_{(s',t')})$ are defined similarly as in Equation 11.

Model parameters involved in the preceding three spatial-temporal energy functions (i.e., $\beta_1, \ldots, \beta_5$ in Equations 10–12) are crucial to the classification, as they determine the importance of different components in the total spatial-temporal energy functions in Equation 9. We estimate these parameters by minimizing the error rates of training data using a genetic algorithm (Tso and Mather 1999; D. S. Liu et al. 2008).

Accuracy Assessment

Accuracy assessment is an integral component of any remote sensing classification and change detection study (Foody 2002; Congalton and Green 2009). For land-cover change detection based on post-classification comparison, accuracy assessment can be performed with both classification results and change detection results. In the case of land-cover classification, accuracy assessment generally follows an error matrix–based approach (Congalton and Green 2009). Specifically, a classification error matrix is first constructed by cross-tabulating the classified land-cover classes at a number of randomly sampled testing pixels against their corresponding ground classes. Then, accuracy measures such as overall accuracy and kappa statistics are calculated from the classification error matrix (Congalton and Green 2009). When multi-temporal land-cover classification is involved, classification accuracy at each date can be assessed independently using a separate classification error matrix for each date (e.g., Mertens and Lambin 2000; Petit, Scudder, and Lambin 2001; F. Yuan et al. 2005).

For land-cover change detection, a rigorous accuracy assessment should also follow an error matrix–based approach similar to the one used for land-cover classification (van Oort 2007; Congalton and Green 2009), but constructing a change detection error matrix is generally challenging due to the difficulties in collecting sufficient testing samples of land-cover changes over time (Congalton and Green 2009). This is particularly true for change detection involving more than two dates in which the number of possible change trajectories is large. In the absence of sufficient testing samples of land-cover change, alternative approaches that do not rely on a change detection error matrix are needed for accuracy assessment of change detection. In this article, two approaches are used to assess the accuracy of land-cover change trajectories. The first approach seeks to estimate the overall accuracy of change detection using classification accuracies at individual dates under two extreme conditions: a pessimistic accuracy and an optimistic accuracy (van Oort 2007). The pessimistic accuracy is simply calculated as the product of overall classification accuracies at individual dates by assuming no temporal correlation among classification

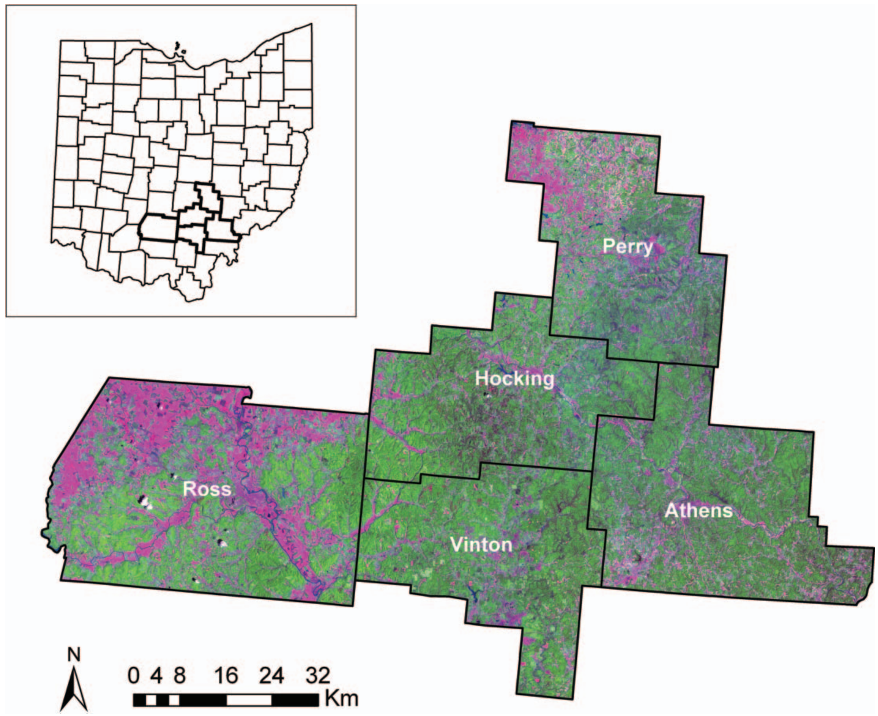

Figure 3. The study area, southeast Ohio, United States. Landsat 5 TM images acquired in 2008 were shown in false color composite (bands 7 + 4 + 2) and clipped to the five-county study area. (Color figure available online.)

errors (D. Yuan, Elvidge, and Lunetta 1998). The optimistic accuracy is determined by the minimum of overall classification accuracies at individual dates with the assumption of maximum positive temporal correlation among classification errors (van Oort 2007). The rationale for this approach lies in the fact that a positive temporal correlation generally exists between classification errors at different dates (Burnicki, Brown, and Goovaerts 2007; D. S. Liu and Chun 2009). Although the actual temporal correlation is unknown, it should be larger than zero (i.e., no correlation) and smaller than one (i.e., maximum positive correlation). Thus, the two extreme accuracy measures together provide a reasonable range for the true change detection accuracy. The second approach is based on the rationality analysis of reconstructed land-cover change trajectories (H. Liu and Zhou 2004). As mentioned earlier, the propagation of classification errors in post-classification comparison could result in illogical land-cover transitions between two consecutive dates (e.g., urban → forest). Given multi-temporal images at m dates, the land-cover change trajectory at each pixel location consists of $m - 1$ land-cover transitions, which can be determined to be logical or illogical based on expert knowledge. Although all $m - 1$ land-cover transitions

Table 1. Summary of satellite images used in the case study

Year	Satellite sensor	Acquisition date	Path/row
1977	Landsat 2 MSS	18 July 1977	20/32,20/33
1983	Landsat 4 MSS	26 June 1983	18/32,18/33
		22 August 1983	19/32,19/33
1988	Landsat 5 TM	8 June 1988	18/32,18/33
		15 June 1988	19/32,19/33
1993	Landsat 5 TM	31 July 1993	18/32,18/33
		9 August 1993	19/32,19/33
1998	Landsat 5 TM	6 July 1998	18/32,18/33
		13 July 1998	19/32,19/33
2003	Landsat 5 TM	25 June 2003	18/32,18/33
		20 July 2003	19/32,19/33
2008	Landsat 5 TM	6 June 2008	18/32,18/33
		17 July 2008	19/32,19/33

Table 2. Illogical land-cover transitions over five-year periods

	To					
From	W	F	C	G	U	M
W	0	1	0	0	0	1
F	0	0	0	0	0	0
C	0	1	0	0	0	0
G	0	0	0	0	0	0
U	1	1	1	0	0	1
M	0	1	0	0	1	0

Note: Land-cover categories: W = water; F = forest (a closed canopy stand of trees); C = crop; G = grass/shrub; U = urban; M = mine (surface mining). The number 1 in the transition matrix indicates an illogical transition (i.e., a transition that is highly unlikely to occur within a five-year interval in the context of the study area).

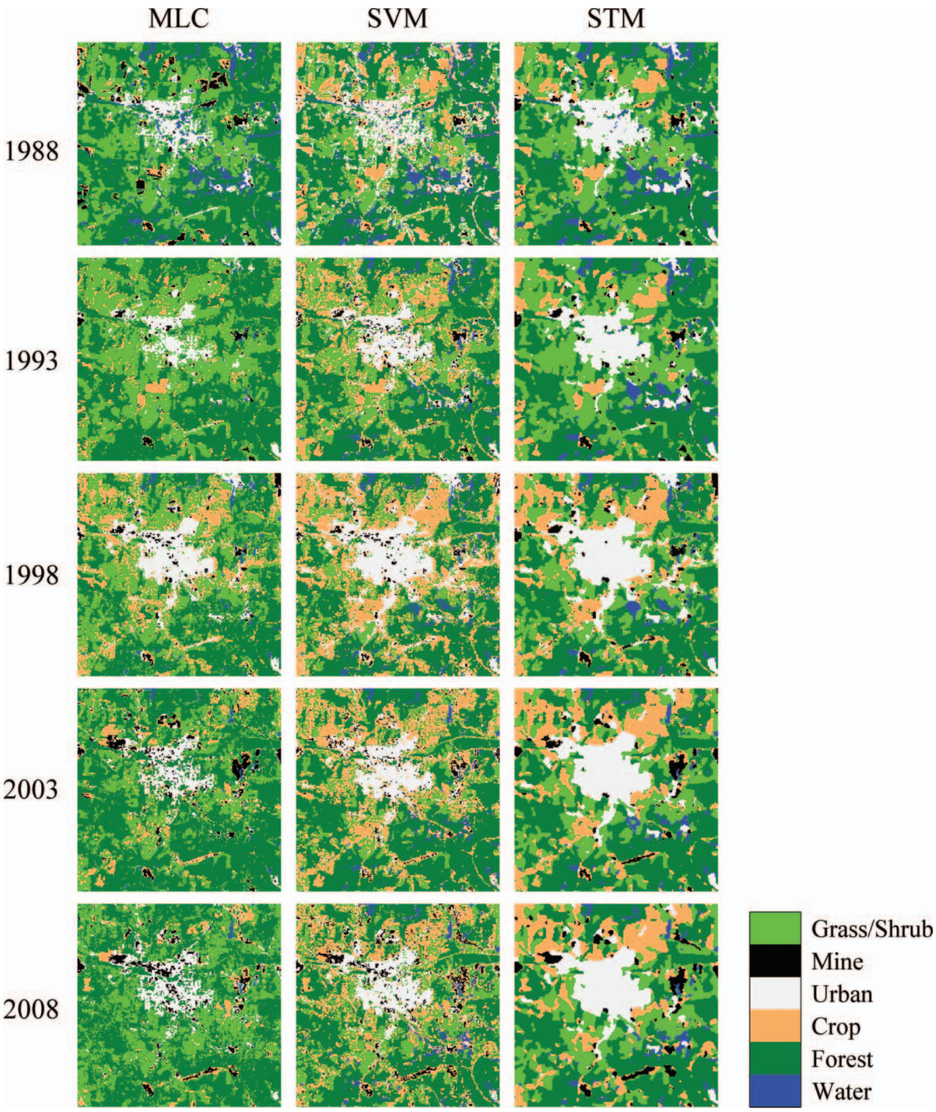

Figure 4. Examples of the land-cover classification maps from 1988 to 2008 clipped to a subset of 200 by 200 pixels for illustration purposes. *Note:* MLC = maximum likelihood classification; SVM = support vector machines; STM = spatial-temporal modeling. (Color figure available online.)

being logical at one pixel location does not necessarily mean that the corresponding land-cover change trajectory is correct, the occurrence of one or more illogical transitions at one pixel location would definitely indicate the presence of errors in the land-cover change trajectory. Therefore, the percentage of illogical land-cover transitions at each of the $m - 1$ time periods and the percentage of illogical land-cover change trajectories over all m dates can be calculated to measure the illogical errors in change detection results.

Case Study

Study Area: Southeast Ohio

The case study focuses on land-cover changes associated with overall forest recovery in southeast Ohio. There, the landscape has been significantly impacted by underground and surface strip mining over the past 120 years. Yet economic shifts and other processes in the region have allowed for the recovery of forests and other vegetation throughout the region, particularly after the 1930s; this was hastened by federal and state government investment in creating state and national forests on eroded agricultural and timber lands (Wilson 1993). Simultaneously, nonforest land cover is also expanding in the region, which serves to fragment, reverse, or accelerate successional processes in unexpected ways (McSweeney and McChesney 2004). The result is a landscape in which the fundamental dynamic trajectories of land-cover change are complex, heterogeneous, and nonlinear patchy in nature. Therefore, Ohio's southeast provides an excellent site for testing our change detection method to identify complex trajectories of land-cover change from time series of satellite imagery.

Table 3. Classification accuracies for all seven years measured in overall accuracy (Overall) and kappa statistics (Kappa)

	MLC		SVM		STM	
Year	Overall (%)	Kappa	Overall (%)	Kappa	Overall (%)	Kappa
1977	77.1	0.657	83.2	0.744	92.5	0.887
1983	77.2	0.663	81.6	0.723	92.0	0.879
1988	86.1	0.793	90.9	0.860	95.3	0.928
1993	80.5	0.707	88.2	0.823	95.7	0.936
1998	86.0	0.789	90.3	0.855	94.8	0.923
2003	81.6	0.724	90.1	0.852	94.2	0.913
2008	80.3	0.745	88.2	0.848	93.6	0.918

Note: MLC = maximum likelihood classification; SVM = support vector machines; STM = spatial-temporal modeling.

The study area includes five contiguous counties within southeast Ohio: Athens, Hocking, Perry, Ross, and Vinton (Figure 3). These five counties were chosen because they are broadly representative of the southeast, capturing the region's range of economic and ecological characteristics (McSweeney and McChesney 2004). Hocking County was one of the first to be completely denuded of forest cover, and today its secondary forests are among the state's oldest. Athens County has more of its land in small farming. Land use in Perry and Vinton counties has traditionally been dominated by mining. Whereas most surface mines in Perry County have been reclaimed and now form part of Wayne National Forest, coal mines remain active in Vinton County (McSweeney and McChesney 2004). Ross County is relatively different from the other four counties, as agriculture has dominated land uses for the last several decades and there is small coverage of forested areas.

Landsat Data and Reference Data

A time series of satellite images acquired from Landsat MSS/TM sensors were downloaded from the USGS Web site with the help of the GloVis (Global Visualization Viewer) tool. The Landsat image time series were distributed at seven time points from 1977 to 2008 with a rough five-year interval (Table 1). All MSS and TM images were processed at Level 1T by the USGS. The spatial resolutions of the Landsat products are 60 m for MSS images and 30 m for TM images. A careful examination indicated that all TM images were accurately aligned with each other. Therefore, image-to-image registration was not performed for TM images. Instead, all MSS images were resampled to 30-m resolution and registered to TM images. The root mean square error (RMSE) for each MSS image was within a half-pixel.

Table 4. Overall accuracy of land-cover change trajectories

	Overall accuracy		
	Pessimistic (%)	Optimistic (%)	Average (%)
MLC	23.2	77.1	50.2
SVM	39.0	81.6	60.3
STM	64.9	92.0	78.5

Note: MLC = maximum likelihood classification; SVM = support vector machines; STM = spatial-temporal modeling.

Based on our knowledge of the study area, a classification scheme of six general land-cover classes was adopted here including water, forest, crop, grass/shrub, urban, and mine, from which the illogical land-cover transitions within a five-year interval were defined based on expert knowledge (Table 2). To facilitate land-cover classification and accuracy assessment, reference land-cover classes were collected at randomly sampled pixels for each of the seven years. Due to the challenge in collecting reference land-cover data over the past thirty-one years, a variety of methods and data sources were explored in the data collection process, including field surveys, visual interpretation of aerial photographs, mine permit maps, and topographic maps. Field surveys were conducted in spring 2009. Aerial photographs in selected areas were acquired through National Aerial Photograph Program (NAPP) for 1983; National High Altitude Photography (NHAP) for the years 1988, 1993, and 1998; and the Ohio Statewide Imagery Program (OSIP) for 2003 and 2008. Mine permit maps in 1988, 1993, 2003, and 2008 were obtained from an annual report on Ohio mineral industries by the Ohio Department of Natural Resources (ODNR). Ohio 7.5-minute series topographic maps were obtained from USGS publications for the years 1977 and 1983. Reference data were randomly split into two independent subsets: One served for training purposes and the other was used for accuracy assessment.

Classification and Change Detection Results

Land-cover maps at seven dates were generated by classifying the Landsat image time series of the study area using the proposed spatial-temporal modeling (STM) approach. Land-cover change trajectories were then constructed from the seven classification maps by multi-temporal post-classification comparison. For the purpose of comparison, land-cover

Table 5. Summary of illogical land-cover transitions resulted in the time series of classification maps

Time period		W→F	W→M	C→F	U→W	U→F	U→C	U→M	M→F	M→U	Total
1977	MLC	0.04	0.00	5.29	0.05	0.55	0.99	0.15	0.08	0.12	7.27
↓	SVM	0.36	0.00	5.56	0.01	0.02	0.10	0.01	0.05	0.04	6.15
1983	STM	0.12	0.00	0.23	0.00	0.00	0.00	0.00	0.03	0.00	0.38
1983	MLC	0.11	0.00	3.06	0.40	1.04	1.06	0.13	0.07	0.13	6.00
↓	SVM	0.04	0.00	4.63	0.07	0.05	0.21	0.01	0.02	0.06	5.08
1988	STM	0.09	0.02	0.55	0.01	0.00	0.00	0.01	0.03	0.06	0.78
1988	MLC	1.85	0.01	1.38	0.02	0.53	1.23	0.07	0.21	0.06	5.36
↓	SVM	1.40	0.01	1.29	0.08	0.75	2.00	0.13	0.01	0.03	5.70
1993	STM	0.64	0.01	0.17	0.02	0.18	0.13	0.04	0.02	0.01	1.23
1993	MLC	0.17	0.00	4.79	0.01	0.11	0.34	0.07	0.02	0.05	5.57
↓	SVM	0.26	0.00	2.73	0.05	0.11	0.71	0.06	0.01	0.17	4.10
1998	STM	0.23	0.01	0.44	0.01	0.04	0.15	0.03	0.01	0.06	0.96
1998	MLC	0.09	0.01	2.89	0.01	0.16	0.19	0.08	0.01	0.08	3.52
↓	SVM	0.27	0.00	2.26	0.04	0.16	0.84	0.11	0.00	0.06	3.76
2003	STM	0.10	0.00	0.33	0.01	0.03	0.06	0.02	0.01	0.02	0.58
2003	MLC	0.05	0.00	1.04	0.07	0.08	0.09	0.11	0.07	0.12	1.63
↓	SVM	0.09	0.00	1.28	0.02	0.04	0.38	0.11	0.00	0.10	2.04
2008	STM	0.03	0.00	0.16	0.00	0.01	0.04	0.01	0.00	0.02	0.28

Note: All numbers are in percentages; 0.00 represents < 0.01. MLC = maximum likelihood classification; SVM = support vector machines; STM = spatial-temporal modeling.

classification and change detection were also conducted using a non-contextual approach based on maximum likelihood classification (MLC). The MLC-based non-contextual approach serves as the benchmark for the proposed STM approach because it represents one of the most widely used methods in current LULCC studies. In addition, given that the proposed spatial-temporal classification was initialized by SVM, land-cover classification and change detection results were also obtained from SVM for additional comparison. As SVM only uses spectral information, the comparison between SVM and the proposed STM approach can reveal the usefulness of spatial-temporal contextual information in mapping land-cover change trajectories.

Due to the large size of the study area, the time series of classification maps over the entire study area cannot be shown here. For illustration purposes, examples of the land-cover classification maps from 1988 to 2008 clipped to a subset of 200 by 200 pixels are shown in Figure 4. It can be seen that more spatial coherence was achieved in the classified maps by the proposed approach (STM) compared with the two non-contextual approaches (MLC and SVM), indicating that the use of spatial-temporal contextual information is effective in reducing the "salt-and-pepper" effect.

Table 6. Summary statistics of the reconstructed land-cover change trajectories

	All change trajectories		Illogical change trajectories	
	Total number	Percentage (%)	Total number	Percentage (%)
MLC	55,150	63.2	40,636	24.9
SVM	51,749	59.1	36,307	23.7
STM	19,775	32.4	10,529	4.0

Note: MLC = maximum likelihood classification; SVM = support vector machines; STM = spatial-temporal modeling.

Classification Accuracy Assessment. Accuracy assessment was performed for all land-cover classification results using reference data at individual dates. Table 3 summarizes the classification accuracies measured by overall accuracy and kappa statistics for all three approaches under comparison. The classification accuracies for the benchmark approach (MLC) were low to moderate and varied greatly within the seven dates, with overall accuracies ranging from 77 percent to 86 percent and kappa statistics from 0.66 to 0.79. In particular, classification accuracies in 1977 and 1983 were considerably lower than those in the later years,

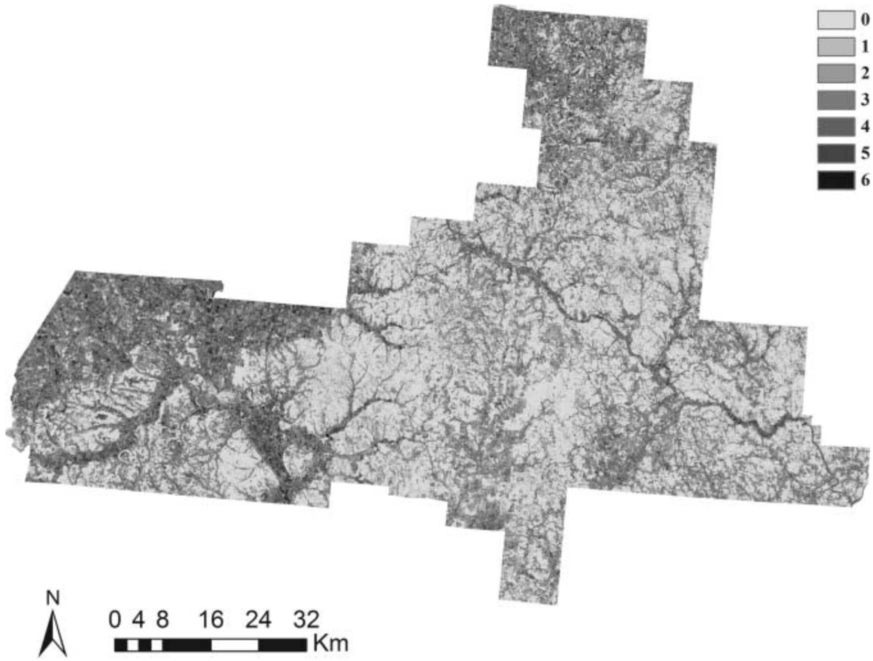

Figure 5. Number of changes over seven dates from maximum likelihood classification (MLC).

which might be due to the lower spatial resolution and fewer spectral bands of MSS images for the first two dates. For the non-contextual classifications based on SVM, the overall accuracies and kappa statistics were moderate and varied from 82 percent to 91 percent and from 0.72 to 0.86, respectively. Similar to MLC, classification accuracies were much lower in 1977 and 1983 than in the later years. By contrast, classification results obtained from the proposed STM approach were consistent and accurate at all dates, with overall accuracies at about 92 percent to 96 percent and kappa statistics at about 0.88 to 0.94. Comparatively, for the two non-contextual classification methods, SVM outperformed MLC with 4 percent to 8 percent higher in overall accuracies and 0.06 to 0.12 higher in kappa statistics. Further improvements on the initial results of SVM were obtained by using spatial-temporal contextual information in STM: Overall accuracies increased by

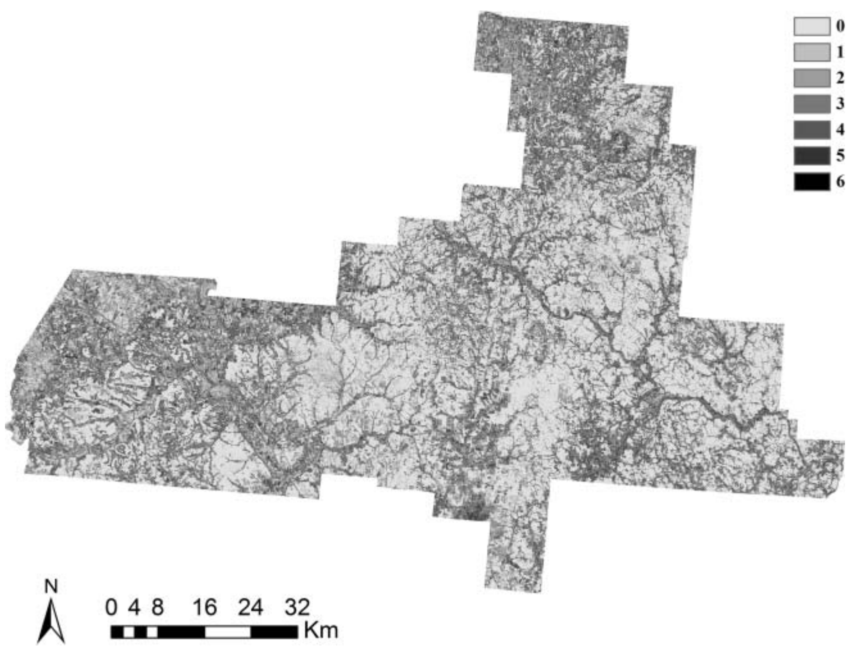

Figure 6. Number of changes over seven dates from support vector machines (SVM).

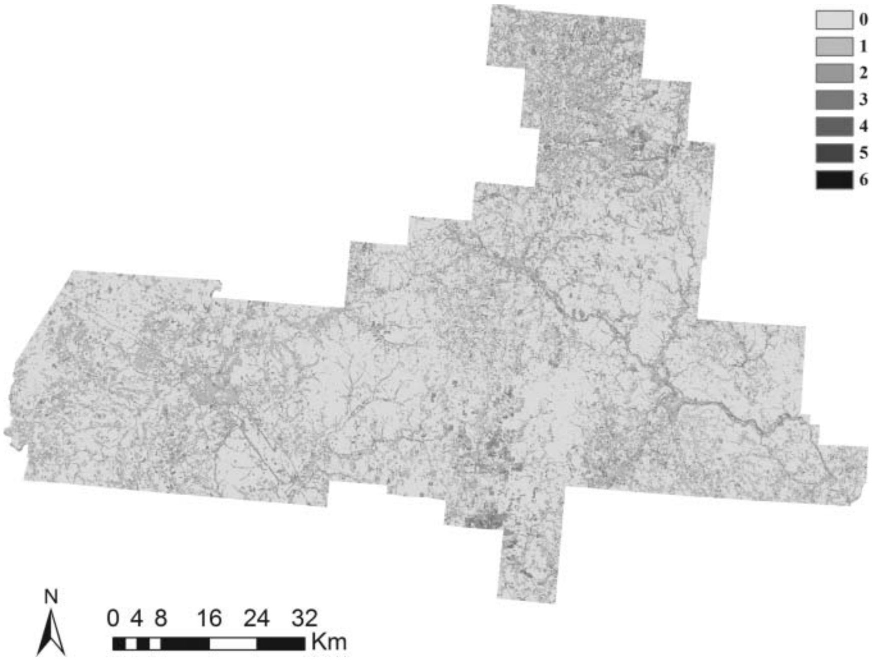

Figure 7. Number of changes over seven dates from spatial-temporal modeling (STM).

4 percent to 10 percent and kappa statistics increased by 0.06 to 0.16. Consequently, significant improvements were achieved by the STM approach over the benchmark approach (MLC): Overall accuracies increased 9 percent to 20 percent and kappa statistics increased 0.14 to 0.27. Moreover, in contrast to MLC and SVM, classification accuracies in 1977 and 1983 were comparable to later years in STM, indicating that the use of spatial-temporal contextual information could compensate for the lower spatial resolution and fewer spectral bands of MSS images.

Change Detection Accuracy Assessment. Based on the classification accuracies in Table 3, the overall accuracies of the resulting land-cover change trajectories were estimated under two extreme conditions (Table 4). First, multiplying the individual overall classification accuracies gave the pessimistic overall change detection accuracy, which was 23.2 percent for MLC, 39.0 percent for SVM, and 64.9 percent for STM. Second, the minimum of the overall classification accuracies at all dates determined the optimistic overall change detection accuracy: 77.1 percent for MLC, 81.6 percent for SVM, and 92.0 percent for STM. In addition, the average of the pessimistic and optimistic accuracies was calculated to represent the middle point of the two extreme conditions, yielding 50.2 percent, 60.3 percent, and 78.5 percent for MLC, SVM, and STM, respectively. Clearly, all of the accuracy measures showed that the land-cover change trajectories reconstructed by the proposed approach (STM) were much more accurate compared with those from the two non-contextual approaches (MLC and SVM). This is consistent with the classification results reported in Table 3, confirming the effectiveness of the spatial-temporal contextual information in reconstructing accurate land-cover change trajectories.

The percentages of the nine illogical land-cover transitions defined in Table 2 are reported for each of the six time periods from 1977 to 2008 (Table 5). For all three approaches, transitions from crop to forest ($C \rightarrow F$) and urban to crop ($U \rightarrow C$) account for most of the illogical transitions. Despite the superior classification performance of SVM over MLC, the percentages of illogical land-cover transitions were comparable between SVM and MLC, indicating that a competitive classifier utilizing only spectral information might not be sufficient to generate temporally consistent land-cover results. In contrast, nearly all illogical land-cover transitions resulting from the proposed approach were significantly less than those from the two non-contextual approaches. This clearly demonstrates the effectiveness of the temporal contextual information (i.e., the temporal exclusion component in STM) in reducing illogical transitions.

Summary of Change Trajectories. Table 6 summarizes several statistics of the resulting land-cover change trajectories, where all change trajectories represent pixels that had changed at least once over the

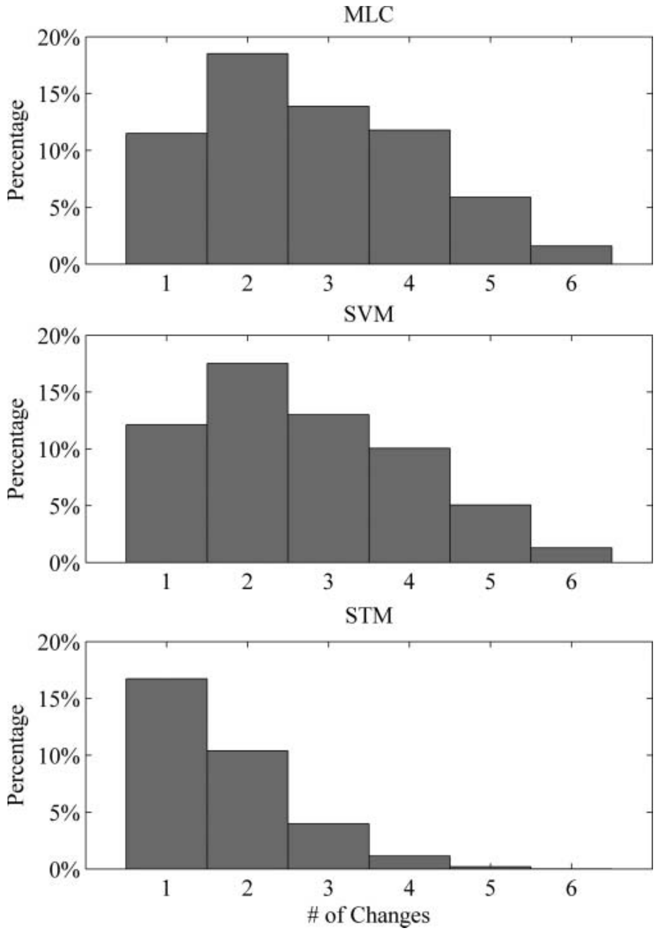

Figure 8. Normalized histogram of change frequency of all change trajectories (i.e., trajectories with at least one land-cover change). The *x* axis represents the number of changes, which ranges from one to six given the seven dates. The *y* axis represents the percentages of pixels experiencing one to six changes. *Note:* MLC = maximum likelihood classification; SVM = support vector machines; STM = spatial-temporal modeling.

seven dates and illogical change trajectories correspond to pixels with at least one illogical transition listed in Table 2. With six land-cover classes and seven dates, the classification results based on MLC and SVM generated more than 50,000 different land-cover change trajectories, the vast majority of which are illogical. The large number of illogical change trajectories can be attributed to the propagation of classification errors. With the use of spatial-temporal information, the total numbers of all and illogical change trajectories were greatly reduced by STM. Nevertheless, it is not possible to validate these statistics without knowing the number of true change trajectories. Therefore, the percentage of all (or illogical) change trajectories (i.e., the area rate of the change trajectories) is compared for further evaluation. Both non-contextual approaches (MLC and SVM) showed that about 60 percent of the study area had changed during the past thirty-one years. This high change rate was unexpected based on expert knowledge of the study area and visual inspection of the Landsat images. The overestimated change rates by MLC and SVM were a typical result of the propagation of classification errors in post-classification comparison (Pontius and Lippitt 2006). In contrast, the overall change rate was dramatically reduced to 32 percent with the proposed approach (STM), demonstrating that the use of spatial-temporal contextual information led to substantial reductions in pseudo-changes due to classification errors. Finally, the illogical land-cover change trajectories from STM accounted for 4 percent of the study area, much smaller than the results obtained from MLC (24.9 percent) and SVM (23.7 percent). This result was consistent with that in Table 5, which further confirmed the usefulness of a temporal exclusion component in reducing illogical change trajectories. It should be mentioned that the percentages of illogical change trajectories in Table 6 are a little smaller than the cumulative sums of total illogical transitions over six time periods reported in Table 5 because one illogical land-cover change trajectory can have more than one illogical transition.

Figures 5 through 7 show the maps of the number of changes (i.e., change frequency) detected at each pixel over seven dates by the three approaches. The two non-contextual approaches (Figure 5 and Figure 6) demonstrate high change frequency throughout the study area, particularly in Ross County and Perry County. In contrast, the STM approach (Figure 7) shows generally lower change frequency. Figure 8 shows the further breakdown of the number of changes over seven dates for all change trajectories (i.e., trajectories with at least one land-cover change). It is clear that MLC and SVM were significantly different from STM in the distribution of change frequencies. Particularly, MLC and SVM estimated that about 30 percent of pixels had changed three times or more over seven dates and 8 percent changed five times or more, whereas the numbers were only 5 percent and 0.2 percent, respectively, according to STM. As the probability of observing a land-cover change trajectory with a high change frequency is generally small (H. Liu and Zhou 2004), the result showed that the two non-contextual approaches not only overestimated the overall change rate but also overestimated the change frequency.

Discussion and Conclusions

Land-cover change, especially over a long time period, often follows a complex pathway that can't be well captured by satellite observations at two dates. Temporal trajectories of land-cover change constructed from satellite images over multiple dates can better characterize the complex nature of land-cover dynamics and thus have the potential to improve our understanding of human–environment adaptive systems. The increasing availability of long time series of satellite images, especially the recent free release of multi-decadal Landsat satellite archives, presents a great opportunity to enhance our ability to monitor land-cover change more frequently and promote the move from traditional bi-temporal change analysis to multi-temporal change trajectory analysis. To achieve this, it is imperative to develop accurate and efficient change detection methods that can take advantage of the increasing temporal depth of satellite images to track the trajectories of land-cover change over time. In this article, we developed one such change detection method and evaluated its performance with a time series of seven Landsat images in southeast Ohio.

One of the most important properties of land cover and land-cover change is its strong dependence over space and time (i.e., spatial autocorrelation and temporal dependence). This dependence structure is fundamental to remote sensing of land-cover classification and change detection because it defines the spatial-temporal context of land-cover dynamics at individual pixels. Despite this fact, most change detection methods do not account for the contextual dependence and thus are non-contextual in nature. The method developed in this article distinguishes itself for its integrated contextual (both spatial and temporal) approach to land-cover change detection. The key innovation lies in the use of MRF theory to model spatial-temporal contextual information explicitly in the classification of time series images. Compared with conventional non-contextual approaches, the contextual approach achieved superior performance in the change detection results in the case study, which demonstrates the critical role of spatial-temporal contextual information in generating accurate and consistent trajectories of land-cover change. Specifically, due to the inherent uncertainty of spectral information in resolving different land-cover classes, land-cover classification based on spectral information alone generally does not conform to its underlying contextual constraints as illustrated by the lack of spatial contiguity (e.g., "salt-and-pepper" effect) and temporal consistency (e.g., illogical land-cover transitions). The use of spatial-temporal information can impose contextual constraints on land-cover results and thus mitigate the impact of spectral uncertainty in classification: (1) spatial contextual constraints tend to increase spatial smoothness (or autocorrelation) of classification results, which can remove speckle errors and thus reduce spurious changes; and (2) temporal contextual constraints can improve the temporal consistency of classification results over multiple dates and reduce illogical land-cover transitions. As a consequence, the resulting land-cover classification becomes more consistent with its spatial-temporal context, which in turn leads to improved accuracy and consistency of change detection results.

Accuracy assessment for change detection is a complex and challenging task. The main difficulty arises from the lack of sufficient reference data to capture a potentially large number of change classes, which prevents the construction of a change detection error matrix. In the case of this study, reference data were only available for land-cover classification at each date but not for change detection over seven dates. For this reason, change detection results were evaluated using two alternative approaches: one based on individual classification accuracies and the other based on the trajectory results themselves. The two approaches provided useful accuracy indicators to compare different change results, which served our purpose of evaluating the proposed change detection method. Nevertheless, it should be acknowledged that the accuracy measures used in the two approaches were not as complete and rigorous as those derived from a change detection error matrix if sufficient reference data on change trajectories are available. For example, both pessimistic accuracy and optimistic accuracy focus only on the overall accuracy of all trajectories, but sometimes it is necessary to assess the accuracy of specific change trajectories (e.g., trajectories related to forest recovery). In addition, although rationality analysis of the change results can identify illogical change trajectories, the accuracy of logical change trajectories remains unknown. Further efforts are needed to improve change detection accuracy assessment.

Land-cover change trajectories are defined in this article as a temporal sequence of land-cover classes observed at multiple dates. This definition is based on a discrete representation of landscape by categorical fields and emphasizes transitions between land-cover classes over multiple dates. In other words, this article focuses on drastic changes in the form of land-cover conversions, the complete replacement of one land-cover class by another (e.g., deforestation and urbanization). Land-cover change also includes another important form called *land-cover modifications*, however, which are associated with more subtle changes within a land-cover class but not drastic changes in its overall classification (e.g., agricultural intensification; Lambin, Geist, and Lepers 2003; Lambin and Linderman 2006). To detect subtle changes within land-cover classes, change detection methods should be based on a continuous representation of land surface attributes at the seasonal and interannual scales (Lambin and Linderman 2006). In this sense, the proposed change detection method is not suitable for detecting subtle changes due to land-cover modifications. Trajectory-based change detection methods (e.g., Kennedy, Cohen, and Schroeder 2007; Huang et al. 2010) might be used to capture the subtle changes based on their unique temporal profile established from time series of satellite data or their continuous derivatives (e.g., vegetation indexes, surface temperature).

In summary, this article presents an advanced change detection method based on post-classification comparison for reconstructing land-cover change trajectories from time series of satellite images. The method differs from the conventional post-classification comparison change detection in that a novel STM approach instead of the commonly used non-contextual approach is developed to improve multi-temporal land-cover classification. When evaluated using a time series of seven Landsat images in a case study of southeast Ohio, the STM approach yielded significantly more reliable trajectories of land-cover change compared with two conventional non-contextual approaches. The results demonstrate the effectiveness of the change detection method in reconstructing land-cover change trajectories and also highlight the utility of spatial-temporal contextual information in improving the accuracy and consistency of land-cover results across space and time. This research has important implications for land change science. The change detection methodology developed in this article is general enough to be readily applicable to other LULCC studies with different satellite data and landscapes. Models based on accurate and consistent land-cover change trajectories can better explain the complex dynamic change processes and allow more reliable projections of future changes.

Acknowledgments

This research received support from the Center for Urban and Regional Analysis (CURA) at The Ohio State University and from the National Science Foundation, Award #1010314, "CNH: Collaborative Research: Explaining Socioecological Resilience Following Collapse: Forest Recovery in Appalachian Ohio." The authors would like to thank Kendra McSweeney, Darla Munroe, Becky Mansfield, and other members of the Appalachian Ohio Forest Research Group for their help. Comments from the editor Mei-Po Kwan and four anonymous reviewers are greatly appreciated.

Notes

1. A subset of pixels, c, is a *clique* if any two different pixels of c are neighbors.
2. $\mathbb{N}_{T_1}(s,t) \equiv \emptyset$ ($\emptyset$ stands for empty set) at $t = 1$ because pixels at the start of the time series have no past temporal neighbors.
3. $\mathbb{N}_{T_2}(s,t) \equiv \emptyset$ at $t = m$ because pixels at the end of the time series have no future temporal neighbors.
4. $U_{T_1} = 0$ at $t = 1$ because pixels at the start of the time series have no past temporal neighbors (i.e., $\mathbb{N}_{T_1}(s,t) \equiv \emptyset$ for $t = 1$).
5. $U_{T_2} = 0$ at $t = m$ because pixels at the end of the time series have no future temporal neighbors (i.e., $\mathbb{N}_{T_2}(s,t) \equiv \emptyset$ for $t = m$).

References

Alves, D. S., and D. L. Skole 1996. Characterizing land cover dynamics using multi-temporal imagery. *International Journal of Remote Sensing* 17 (4): 835–39.

An, L., and D. Brown. 2008. Survival analysis in land change science: Integrating with GIScience to address temporal complexities. *Annals of the Association of American Geographers* 98 (2): 323–44.

Besag, J. 1986. On the statistical analysis of dirty pictures. *Journal of the Royal Statistical Society Series B-Methodological* 48 (3): 259–302.

Boucher, A., K. C. Seto, and A. G. Journel. 2006. A novel method for mapping land cover changes: Incorporating time and space with geostatistics. *IEEE Transactions on Geoscience and Remote Sensing* 44 (11): 3427–35.

Braimoh, A. K., and P. L. G. Vlek. 2005. Land-cover change trajectories in Northern Ghana. *Environmental Management* 36 (3): 356–73.

Burnicki, A. C., D. G. Brown, and P. Goovaerts. 2007. Simulating error propagation in land-cover change analysis: The implications of temporal dependence. *Computers, Environment and Urban Systems* 31 (3): 282–302.

Cohen, W. B., and S. N. Goward. 2004. Landsat's role in ecological applications of remote sensing. *Bioscience* 54 (6): 535–45.

Congalton, R. G., and K. Green. 2009. *Assessing the accuracy of remotely sensed data: Principles and practices*. Boca Raton, FL: CRC Press/Taylor & Francis.

Coppin, P., I. Jonckheere, K. Nackaerts, B. Muys, and E. Lambin. 2004. Digital change detection methods in ecosystem monitoring: A review. *International Journal of Remote Sensing* 25 (9): 1565–96.

Cressie, N. 1993. *Statistics for spatial data*. Revised ed. New York: Wiley.
Dubes, R. C., and A. K. Jain. 1989. Random field models in image analysis. *Journal of Applied Statistics* 16 (2): 131–64.
Foley, J. A., R. DeFries, G. P. Asner, C. Barford, G. Bonan, S. R. Carpenter, F. S. Chapin, et al. 2005. Global consequences of land use. *Science* 309 (5734): 570–74.
Foody, G. M. 2002. Status of land cover classification accuracy assessment. *Remote Sensing of Environment* 80 (1): 185–201.
Goward, S. N., and D. L. Williams. 1997. Landsat and Earth systems science: Development of terrestrial monitoring. *Photogrammetric Engineering and Remote Sensing* 63 (7): 887–900.
Hammersley, J., and P. Clifford. 1971. Markov fields on finite graphs and lattices. Unpublished manuscript, Oxford University.
Huang, C., S. Goward, J. Masek, N. Thomas, Z. Zhu, and J. Vogelmann. 2010. An automated approach for reconstructing recent forest disturbance history using dense Landsat time series stacks. *Remote Sensing of Environment* 114 (1): 183–98.
Kennedy, R. E., W. B. Cohen, and T. A. Schroeder. 2007. Trajectory-based change detection for automated characterization of forest disturbance dynamics. *Remote Sensing of Environment* 110 (3): 370–86.
Kuemmerle, T., O. Chaskovskyy, J. Knorn, V. C. Radeloff, I. Kruhlov, W. S. Keeton, and P. Hostert. 2009. Forest cover change and illegal logging in the Ukrainian Carpathians in the transition period from 1988 to 2007. *Remote Sensing of Environment* 113 (6): 1194–1207.
Lambin, E. F. 1997. Modelling and monitoring land-cover change processes in tropical regions. *Progress in Physical Geography* 21 (3): 375–93.
Lambin, E., X. Baulies, N. Bockstael, G. Fischer, T. Krug, R. Leemans, E. Moran, R. Rindfuss, Y. Sato, and D. Skole. 1999. Land-use and land-cover change (LUCC): Implementation strategy. IGBP Report No. 48 and IHDP Report No. 10, ed. C. Nunes and J. I. Augé. Stockholm, Sweden: IGBP Secretariat.
Lambin, E. F., H. J. Geist, and E. Lepers. 2003. Dynamics of land-use and land-cover change in tropical regions. *Annual Review of Environment and Resources* 28:205–41.
Lambin, E. F., and M. Linderman. 2006. Time series of remote sensing data for land change science. *IEEE Transactions on Geoscience and Remote Sensing* 44 (7): 1926–28.
Li, S. Z. 2001. *Markov random field modeling in image analysis*. Tokyo: Springer.
Liu, D. S., and Y. W. Chun. 2009. The effects of different classification models on error propagation in land cover change detection. *International Journal of Remote Sensing* 30 (20): 5345–64.
Liu, D. S., M. Kelly, and P. Gong. 2006. A spatial-temporal approach to monitoring forest disease spread using multitemporal high spatial resolution imagery. *Remote Sensing of Environment* 101 (2): 167–80.
Liu, D. S., K. Song, J. R. G. Townshend, and P. Gong. 2008. Using local transition probability models in Markov random fields for forest change detection. *Remote Sensing of Environment* 112 (5): 2222–31.
Liu, H., and Q. Zhou. 2004. Accuracy analysis of remote sensing change detection by rule-based rationality evaluation with post-classification comparison. *International Journal of Remote Sensing* 25 (5): 1037–50.
Lu, D., P. Mausel, E. Brondizio, and E. Moran. 2004. Change detection techniques. *International Journal of Remote Sensing* 25 (12): 2365–2407.
Lucas, R. M., M. Honzak, G. M. Foody, P. J. Curran, and C. Corves. 1993. Characterizing tropical secondary forests using multi-temporal Landsat sensor imagery. *International Journal of Remote Sensing* 14 (16): 3061–67.
Lunetta, R. S., J. F. Knight, J. Ediriwickrema, J. G. Lyon, and L. D. Worthy. 2006. Land-cover change detection using multi-temporal MODIS NDVI data. *Remote Sensing of Environment* 105 (2): 142–54.
McSweeney, K., and R. McChesney. 2004. Outbacks: The popular construction of an emergent landscape. *Landscape Research* 29 (1): 31–56.
Melgani, F., and S. B. Serpico. 2003. A Markov random field approach to spatio-temporal contextual image classification. *IEEE Transactions on Geoscience and Remote Sensing* 41 (11): 2478–87.
Mena, C. F. 2008. Trajectories of land-use and land-cover in the northern Ecuadorian Amazon: Temporal composition, spatial configuration, and probability of change. *Photogrammetric Engineering and Remote Sensing* 74 (6): 737–51.
Mertens, B., and E. F. Lambin. 2000. Land-cover-change trajectories in southern Cameroon. *Annals of the Association of American Geographers* 90 (3): 467–94.
Meyer, W. 1994. *Changes in land use and land cover: A global perspective*. Cambridge, UK: Cambridge University Press.
Myneni, R. B., C. D. Keeling, C. J. Tucker, G. Asrar, and R. R. Nemani. 1997. Increased plant growth in the northern high latitudes from 1981 to 1991. *Nature* 386 (6626): 698–702.
Petit, C., T. Scudder, and E. Lambin. 2001. Quantifying processes of land-cover change by remote sensing: Resettlement and rapid land-cover changes in south-eastern Zambia. *International Journal of Remote Sensing* 22 (17): 3435–56.
Pontius, R., and C. Lippitt. 2006. Can error explain map differences over time? *Cartography and Geographic Information Science* 33 (2): 159–71.
Powell, S. L., W. B. Cohen, Z. Yang, J. D. Pierce, and M. Alberti. 2008. Quantification of impervious surface in the Snohomish water resources inventory area of western Washington from 1972–2006. *Remote Sensing of Environment* 112 (4): 1895–1908.
Rindfuss, R. R., S. J. Walsh, B. L. Turner, J. Fox, and V. Mishra. 2004. Developing a science of land change: Challenges and methodological issues. *Proceedings of the National Academy of Sciences of the United States of America* 101 (39): 13976–81.
Singh, A. 1989. Review article: Digital change detection techniques using remotely-sensed data. *International Journal of Remote Sensing* 10 (6): 989–1003.
Solberg, A. H. S., T. Taxt, and A. K. Jain. 1996. A Markov random field model for classification of multisource satellite imagery. *IEEE Transactions on Geoscience and Remote Sensing* 34 (1): 100–13.
Southworth, J., H. Nagendra, L. A. Carlson, and C. Tucker. 2004. Assessing the impact of Celaque National Park on forest fragmentation in western Honduras. *Applied Geography* 24 (4): 303–22.
Steffen, W., A. Sanderson, P. D. Tyson, J. Jager, P. A. Matson, B. I. Moore, F. Oldfield, K. Richardson, H. J. Schellnhuber, B. L. I. Turner, and R. J. Wasson. 2004.

Global change and the Earth system: A planet under pressure. Berlin: Springer.

Townsend, P. A., D. P. Helmers, C. C. Kingdon, B. E. McNeil, K. M. deBeurs, and K. N. Eshleman. 2009. Changes in the extent of surface mining and reclamation in the central Appalachians detected using a 1976–2006 Landsat time series. *Remote Sensing of Environment* 113 (1): 62–72.

Tso, B. C. K., and P. M. Mather. 1999. Classification of multisource remote sensing imagery using a genetic algorithm and Markov random fields. *IEEE Transactions on Geoscience and Remote Sensing* 37 (3): 1255–60.

Turner, B. L. I., W. C. Clark, R. W. Kates, J. F. Richards, J. T. Mathews, and W. B. Meyer., eds. 1990. *The Earth as transformed by human action: Global and regional changes in the biosphere over the past 300 years*. Cambridge, UK: Cambridge University Press.

Turner, B. L., E. F. Lambin, and A. Reenberg. 2007. The emergence of land change science for global environmental change and sustainability. *Proceedings of the National Academy of Sciences of the United States of America* 104 (52): 20666–71.

U.S. Geological Survey (USGS). 2003. *Landsat: A global land-observing program*. *USGS Fact Sheet 023-03*. Washington, DC: U.S. Geological Survey and U.S. Department of the Interior.

———. 2008. Imagery for everyone. Technical announcement, U.S. Geological Survey and U.S. Department of the Interior. http://landsat.usgs.gov/documents/USGS_Landsat_Imagery_Release.pdf (last accessed 5 February 2011).

Vågen, T. G. 2006. Remote sensing of complex land use change trajectories—A case study from the highlands of Madagascar. *Agriculture Ecosystems & Environment* 115 (1–4): 219–28.

van Oort, P. A. J. 2007. Interpreting the change detection error matrix. *Remote Sensing of Environment* 108 (1): 1–8.

Vitousek, P. M., H. A. Mooney, J. Lubchenco, and J. M. Melillo. 1997. Human domination of Earth's ecosystems. *Science* 277 (5325): 494–99.

Williams, D. L., S. Goward, and T. Arvidson. 2006. Landsat: Yesterday, today, and tomorrow. *Photogrammetric Engineering and Remote Sensing* 72 (10): 1171–78.

Wilson, G. E. 1993. *A development program for the Ohio Valley Region*. Columbus: Ohio Department of Development.

Yuan, D., C. D. Elvidge, and R. S. Lunetta. 1998. Survey of multispectral methods for land cover change analysis. In *Remote sensing change detection: Environmental monitoring methods and applications*, ed. R. S. Lunetta and C. Elvidge, 21–39. Chelsea, MI: Ann Arbor Press.

Yuan, F., K. E. Sawaya, B. C. Loeffelholz, and M. E. Bauer. 2005. Land cover classification and change analysis of the Twin Cities (Minnesota) metropolitan area by multitemporal Landsat remote sensing. *Remote Sensing of Environment* 98 (2–3): 317–28.

Correspondence: Department of Geography, The Ohio State University, 1036 Derby Hall, 154 North Oval Mall, Columbus, OH 43210–1361, e-mail: liu.738@osu.edu (Liu); cai.80@buckeyemail.osu.edu (Cai).